scientific reports

OPEN

Low-intensity pulsed ultrasound combined with microbubble mediated JNK/c-Jun pathway to reverse multidrug resistance in triple-negative breast cancer

Nina Qu[1,6], Zhihui Wu[2,6], Qingkai Meng[3], Menglu Bi[3], Hexiu Liu[4], Xiaoli Cao[1✉] & Yanqing Liu[5]

To investigate the effects of low-intensity pulsed ultrasound combined with microbubble (LIPUS-MB) mediated JNK/c-Jun pathway reversal on multidrug resistance in triple-negative breast cancer and the underlying mechanisms. An orthogonal experiment was designed to screen for the optimal parameters of LIPUS-MB in MDA-MB-231/DOX cells. The CCK-8 assay was used to determine the drug resistance of the cells and to measure their proliferation activity and resistance reversal efficiency at the optimal parameters. Hoechst 33,342 staining and Annexin V-FITC/PI staining were employed to detect cell morphological changes and apoptosis, respectively. The MDA-MB-231/DOX models of transplanted tumor were established in BALB/c. The impact of LIPUS-MB on allograft tumor growth was observed in vivo. Immunohistochemistry was employed to investigate the expression of P-gp, ABCG2, and Ki-67 in tumor tissues, while western blot was utilized to assess the protein expression of P-gp, ABCG2, JNK, p-JNK, c-Jun, p-c-Jun, Bcl-2 and Bax in both MDA-MB-231/DOX cells and allograft tumor tissues. The optimal LIPUS-MB parameters for MDA-MB-231/DOX cells are the microbubble concentration of 20%, ultrasound intensity of $1.0\,W/cm^2$, and irradiation time of 60 s. The drug resistance index of MDA-MB-231/DOX cells is 19.17. Following the optimal parameter application, the IC_{50} value of the cells decreases by 5.71-fold, with a reversal efficiency of 87.03%, and a simultaneous decrease in cell proliferation activity. Compared with other groups, the DOX + LIPUS-MB group displayed the highest incidence of apoptotic nuclear morphology, and the greatest quantity of cellular apoptosis and the most pronounced decrease in the expression levels of P-gp, ABCG2, p-JNK, p-c-Jun, and Bcl-2 proteins within the cells. Conversely, the expression levels of Bax proteins reach the highest levels (all $P < 0.05$). Furthermore, in vivo subcutaneous tumor transplantation experiments in nude mice revealed that the DOX + LIPUS-MB group exhibited smaller tumor growth rate, volume and the expression of P-gp, ABCG2, and Ki-67 compared to the DOX + LIPUS group, indicating the most pronounced inhibitory effect on tumor growth and it significantly inhibited tumor proliferation, promoted its apoptosis. In conclusion, following parameter optimization, LIPUS-MB was found to reduce the drug resistance of MDA-MB-231/DOX cells. The underlying mechanism may involve the downregulation of P-gp and ABCG2 proteins expression through the modulation of the JNK/c-Jun pathway by LIPUS-MB, thereby inhibiting cell proliferation activity and promoting apoptosis, and enhancing the in vivo anti-tumor effect of DOX, thus reversing multidrug resistance in triple-negative breast cancer.

[1]Department of Ultrasound Medicine, Yantai Yuhuangding Hospital, Yantai 264000, China. [2]Department of Vascular Ultrasound, Xiongan Xuanwu Hospital, Xiongan New Area 071702, China. [3]School of Medical Imaging, Binzhou Medical University, Yantai 264003, China. [4]School of Medical Imaging, Weifang Medical University, Weifang 261021, China. [5]Department of Breast Surgery, Yantai Yuhuangding Hospital, Yantai 264000, China. [6]These authors contributed equally to this work. ✉email: xiaolic969@163.com

Global cancer statistics show that breast cancer has surpassed lung cancer to become the most prevalent malignant tumor globally in 2023[1]. As a distinct pathological subtype of breast cancer, triple-negative breast cancer (TNBC) accounts for 10–20% of all breast cancer cases. TNBC is characterized by its strong invasive and metastatic capabilities, posing significant therapeutic challenges and resulting in poor patient prognosis[2]. The absence of human epidermal growth factor receptor 2, estrogen receptor, and progesterone receptor gene expression in TNBC limits the efficacy of endocrine and targeted therapies. Currently, chemotherapy remains the primary treatment modality for TNBC. Doxorubicin (DOX), as an anthracycline drug, demonstrates significant efficacy in the neoadjuvant chemotherapy of TNBC. However, in the advanced stages of treatment, tumor cells often develop multidrug resistance (MDR) to doxorubicin, greatly compromising the efficacy of chemotherapy[3]. Therefore, the search for effective chemotherapy regimens for TNBC treatment and the overcoming of tumor MDR hold paramount significance.

MDR in breast cancer refers to the phenomenon where breast cancer cells upon exposure to a chemotherapeutic agent, subsequently develop resistance to multiple structurally diverse and mechanistically distinct drugs, thus constituting a primary cause of treatment failure[4]. The formation of MDR in breast cancer is intricately complex, involving a myriad of distinct mechanisms such as drug efflux, DNA damage repair, tumor microenvironment, autophagy, alterations in target molecules, and lipid metabolism. The overexpression of ATP-binding cassette (ABC) transporter in cancer cells involved in drug efflux is the most relevant mechanism for MDR. The human genome harbors 48 genes encoding ABC proteins, which are categorized into seven subfamilies, from ABCA to ABCG. Studies have revealed that under the energy supply of ATP, ABC transporters pump drugs out of the cells, diminishing the intracellular drug accumulation and thus diminishing the efficacy of drug treatment, leading to the failure of tumor therapy[5]. Within the family of ABC transporters, P-glycoprotein (P-gp/ABCB1) and breast cancer resistance protein (BCRP/ABCG2) are closely associated with the development of MDR in breast cancer[6]. Although numerous studies have demonstrated that inhibitors of ABC transporters can alleviate or reverse MDR in breast cancer, the specificity, toxic side effects, and drug interactions of these inhibitors constrain their application.

Low-intensity pulsed ultrasound (LIPUS) is a form of ultrasound with an acoustic intensity of less than 3 W/cm^2, output in pulsed wave mode. Its primary mechanism of action involves non-thermal effects (mechanical and cavitation effects), providing non-invasive physical stimulation for therapeutic applications[7]. Additionally, as artificial cavitation nuclei, microbubbles (MB) can significantly enhance the non-thermal effects, and the resulting microjet and shear stress can destroy the vessel wall and the cell membrane around the cavitation core, and generate some temporary transient micropores in the cell membrane, known as sonoporation. This phenomenon increase the permeability of blood vessels and cell membranes and enhance the transfection rate of drugs. In recent years, LIPUS has achieved significant advancements in inducing apoptosis in tumor cells and altering cellular permeability. It is considered a safe and effective method in medical treatment, characterized by high specificity, low systemic toxicity, and minimal side effects. Currently, ultrasound therapy in the field of tumor chemotherapy often involves the use of ultrasound in combination with MB destruction technology to deliver chemotherapeutic drugs to tumor tissues, thereby increasing the intracellular drug concentration and enhancing the cytotoxic effects on tumor cells. Previous studies[9–11] have reported that the combination of LIPUS and MB can target the delivery of anticancer drugs, improve cellular uptake of drugs, and induce apoptosis in various tumor cells, including pancreatic cancer cells, liver cancer cells, and breast cancer cells, thereby inhibiting the growth of cancer cells. However, there are few research on whether LIPUS-MB can increase the efficacy of drug sensitivity in vivo, and the mechanism of LIPUS-MB reversing MDR in TNBC. Therefore, this study aims to explore the effects of LIPUS-MB on MDA-MB-231/DOX cells and to investigate the mechanisms involved in reversing DOX multidrug resistance in TNBC through the design of in vitro cellular experiments and in vivo animal studies, thereby validating our previous hypotheses (Fig. 1). This research aspires to provide new theoretical foundations for the precise treatment of TNBC.

Results

Optimal parameters for LIPUS-MB in MDA-MB-231/DOX cells

An orthogonal experimental design was employed to assess the intracellular transport of FD500 under different parameter combinations using flow cytometry, thereby elucidating the sonoporation effects in cells following each parameter treatment. The experimental setup of the cell culture experients is in Fig. 2a. Subsequently, the cell viability after treatment with corresponding parameter combinations was determined using the CCK-8 assay (Fig. 2b). Through comprehensive analysis of K_{jm}, k_{jm}, and R values, the optimal parameters for LIPUS-MB in MDA-MB-231/DOX cells were determined to be as follows: microbubble concentration of 20%, ultrasound intensity of 1.0 W/cm^2, and ultrasound exposure time of 60s. Under the optimal parameter combination, the sonoporation effect in cells was $65.01 \pm 8.27\%$, and the cell viability was $84.52 \pm 7.97\%$

Drug resistance of MDA-MB-231/DOX cells and the effect of LIPUS-MB on cell drug resistance and proliferative activity

As observed under a 10× magnification, DOX significantly inhibited the growth of MDA-MB-231 cells at lower concentrations (Fig. 2c), a phenomenon not observed in the MDA-MB-231/DOX cell group (Fig. 2d). The IC$_{50}$ value for MDA-MB-231 cells was 1.85μM, while for MDA-MB-231/DOX cells, it was 35.47μM. As shown in Fig. 2e, the drug resistance index for MDA-MB-231/DOX cells was 19.17. Furthermore, following LIPUS-MB treatment, MDA-MB-231/DOX cells exhibited significant cytotoxicity, with an IC$_{50}$ of 6.21μM, markedly lower than the untreated group (35.47μM). The reversal of drug resistance index was 5.71, with a relative drug resistance reversal efficiency of 87.03%, demonstrating the remarkable therapeutic efficacy of LIPUS-MB in inhibiting cell proliferation and reversing MDR.
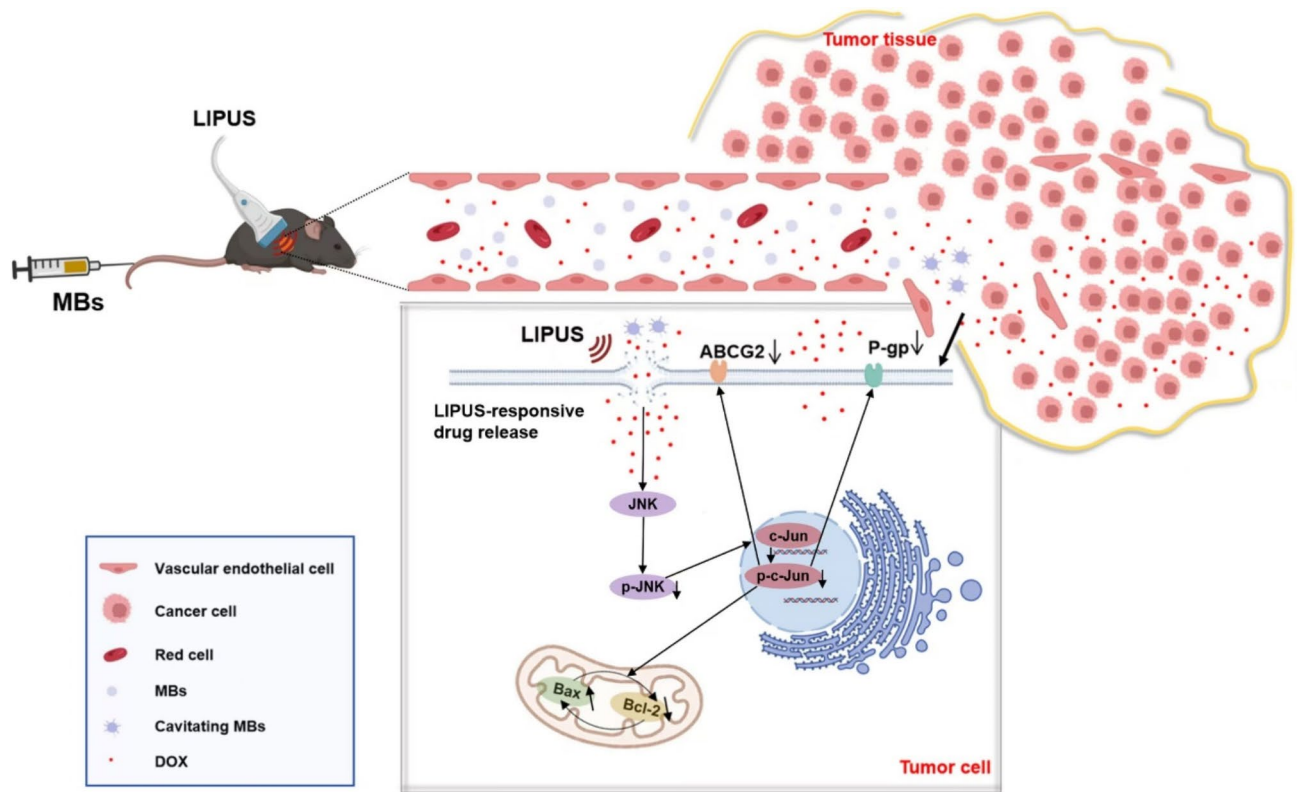
Fig. 1. The schematic of LIPUS-MB reversing TNBC drug resistance, showing drugs penetrating the sonoporated cell membrane, triggering the JNK pathway, inhibiting resistance proteins, and ultimately reversing multidrug resistance in tumor cells to a certain degree.

Influence of LIPUS-MB on the morphology of MDA-MB-231/DOX cells

Following Hoechst33342 staining, NC and DOX groups exhibited uniformly distributed cells with low-intensity fluorescence of normal nuclear morphology. In the LIPUS-MB group, only a few cell nuclei appeared condensed, displaying intensely stained high-intensity fluorescence. The DOX + LIPUS group revealed a higher number of condensed cell nuclei with intensely stained high-intensity fluorescence, and a few nuclei exhibited wrinkling and rupture, displaying bright blue fluorescence, indicative of pronounced apoptotic nuclear changes. In the DOX + LIPUS-MB group, the majority of cell nuclei appeared significantly wrinkled and fragmented, with bright blue-stained nuclei and condensed, marginalized chromatin, demonstrating a stronger apoptotic nuclear morphology alteration (Fig. 2f).

The effects of LIPUS-MB on apoptosis in MDA-MB-231/DOX cells

The results obtained from flow cytometry analysis revealed that the apoptosis rates of the different groups were as follows (Fig. 2g): NC group (12.03 ± 0.67)%, DOX group (15.09 ± 1.05)%, LIPUS-MB group (19.71 ± 1.82)%, DOX + LIPUS group (28.96 ± 1.73)%, and DOX + LIPUS-MB group (48.82 ± 5.28)%. As depicted in Fig. 2h, compared to NC group, the apoptosis rates of the LIPUS-MB, DOX + LIPUS, and DOX + LIPUS-MB groups were all increased (all $P < 0.05$). Furthermore, the apoptosis rate of the DOX + LIPUS group was higher than that of the NC and DOX groups $(P < 0.05)$. Notably, the DOX + LIPUS-MB group exhibited the highest apoptosis rate, with statistically significant differences compared to all other groups (all $P < 0.05$).

Impact of LIPUS-MB on the expression of drug resistance, pathways and apoptosis protein expression in MDA-MB-231/DOX cells

The Western blot results (Fig. 3a) demonstrate that compared with NC group, the protein expression levels of P-gp and ABCG2 were down-regulated in LIPUS-MB group($P < 0.05$);compared to the DOX and LIPUS-MB groups, the DOX + LIPUS-MB groups were able to downregulate the expression levels of P-gp, ABCG2, p-JNK, p-c-Jun, and Bcl-2 proteins, while upregulating the expression levels of Bax proteins (all $P < 0.05$). Furthermore, when comparing the DOX + LIPUS and DOX + LIPUS-MB groups, it was evident that the DOX + LIPUS-MB group exhibited the most significant decrease in P-gp, ABCG2, p-JNK, p-c-Jun, and Bcl-2 protein expression levels, along with the highest levels of Bax protein expression $(P < 0.05)$. Meanwhile, the expression of JNK and c-Jun proteins showed no significant differences among the groups $(P > 0.05)$, suggesting that LIPUS-MB may lead to the down-regulation of P-gp and ABCG2 in MDA-MB-231/DOX cells and promote apoptosis through the JNK/c-Jun pathway. In addition, the effect of LIPUS-MB on JNK/c-Jun signaling pathway was reversed by an appropriate concentration of Ani (0.05 μM). Western blot results showed that the protein expression

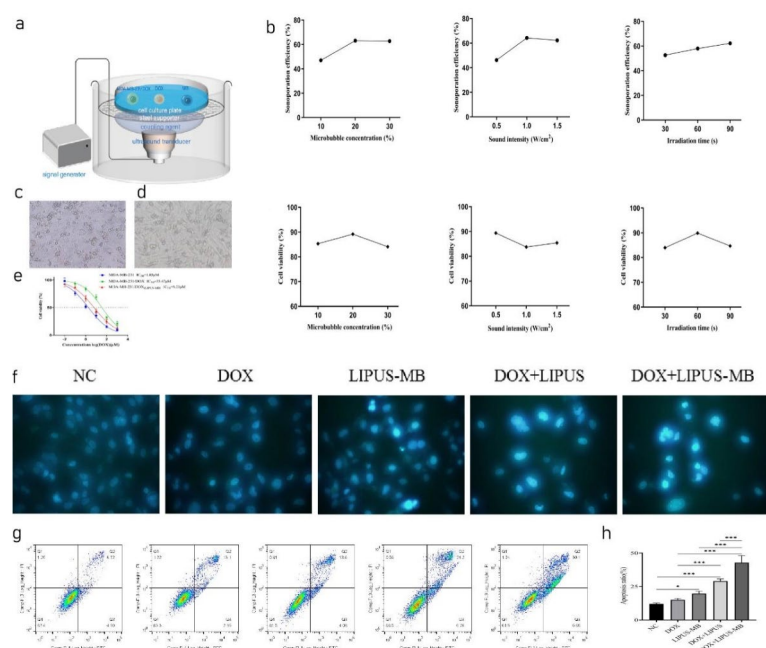Fig. 2. (**a**) The experimental setup of the cell culture experiments. (**b**) The effect of microbubble concentration, ultrasonic intensity and ultrasonic irradiation time on cell acoustic pore effect and cell survival rate, respectively. (**c**) Cell morphology of MDA-MB-231 at 5μM DOX concentration. (**d**) Cell morphology of MDA-MB-231/DOX at 5μM DOX concentration. (**e**) Drug inhibition fitting curve of MDA-MB-231/DOX cells. (**f**) Effect of LIPUS-MB on the karyotype of MDA-MB-231/DOX cells. (**g**) Effect of LIPUS-MB on apoptosis of MDA-MB-231/DOX cells. (**h**) Cell apoptosis rate histogram in each group. $N = 3$, * $P < 0.05$, *** $P < 0.001$ (Table 1).

Factors			Results	
Microbubble concentration(%)	Sound intensity(W/cm^2)	Irradiation time (s)	Sonoporation efficiency (%)	Cell survival rate (%)
20	1.0	60	65.01 ± 8.27	84.52 ± 7.97

Table 1. The optimal experimental parameter combination and results for MDA-MB-231/DOX cell lines.

levels of p-gp, ABCG2, p-JNK, p-c-Jun and Bcl-2 in the DOX + LIPUS-MB group were higher than those in the DOX + LIPUS-MB group, and the protein expression level of Bax in the DOX + LIPUS-MB group was lower than that in the DOX + LIPUS-MB group (all $P < 0.05$). (Fig. 3b)

Effects of LIPUS-MB on subcutaneous transplantation tumor growth and expression of P-gp, ABCG2, and Ki67 in nude mice

Maintain and establish BALB/c nude mice bearing xenografts. Thirty mice were selected and grouped according to tumor volume, ensuring no significant differences in total tumor volume between the two groups. During the treatment process, no accidental deaths occurred among the experimental animals, and the skin surface of all transplanted tumors remained intact, without any ulcers or defects. The tumor volumes in all experimental groups increased steadily throughout the procedure. However, the growth rates and weight of the tumors in the DOX + LIPUS-MB group was significantly lower than those in the DOX and LIPUS-MB groups. Additionally, the volumes of the transplanted tumors in the DOX + LIPUS-MB group was smaller than those in the DOX and LIPUS-MB groups (Fig. 4). Notably, the inhibitory effect was most pronounced in the DOX + LIPUS-MB group ($P < 0.05$), indicating that LIPUS-MB can significantly suppress tumor growth. Furthermore, immunohistochemical analysis revealed that compared to the DOX group, the expression of P-gp, ABCG2, and Ki-67 was reduced in the LIPUS-MB, DOX + LIPUS and DOX + LIPUS-MB groups, with the most significant decrease observed in the DOX + LIPUS-MB group ($P < 0.05$). In contrast, the DOX + LIPUS-MB + Anisomycin group showed an increase in the expression of P-gp, ABCG2, and Ki-67-positive cells compared to the DOX + LIPUS-MB group ($P < 0.05$), indicating that LIPUS-MB downregulates the expression of drug-resistant proteins, thereby inhibiting the proliferative capacity of the tumors. (Fig. 5)
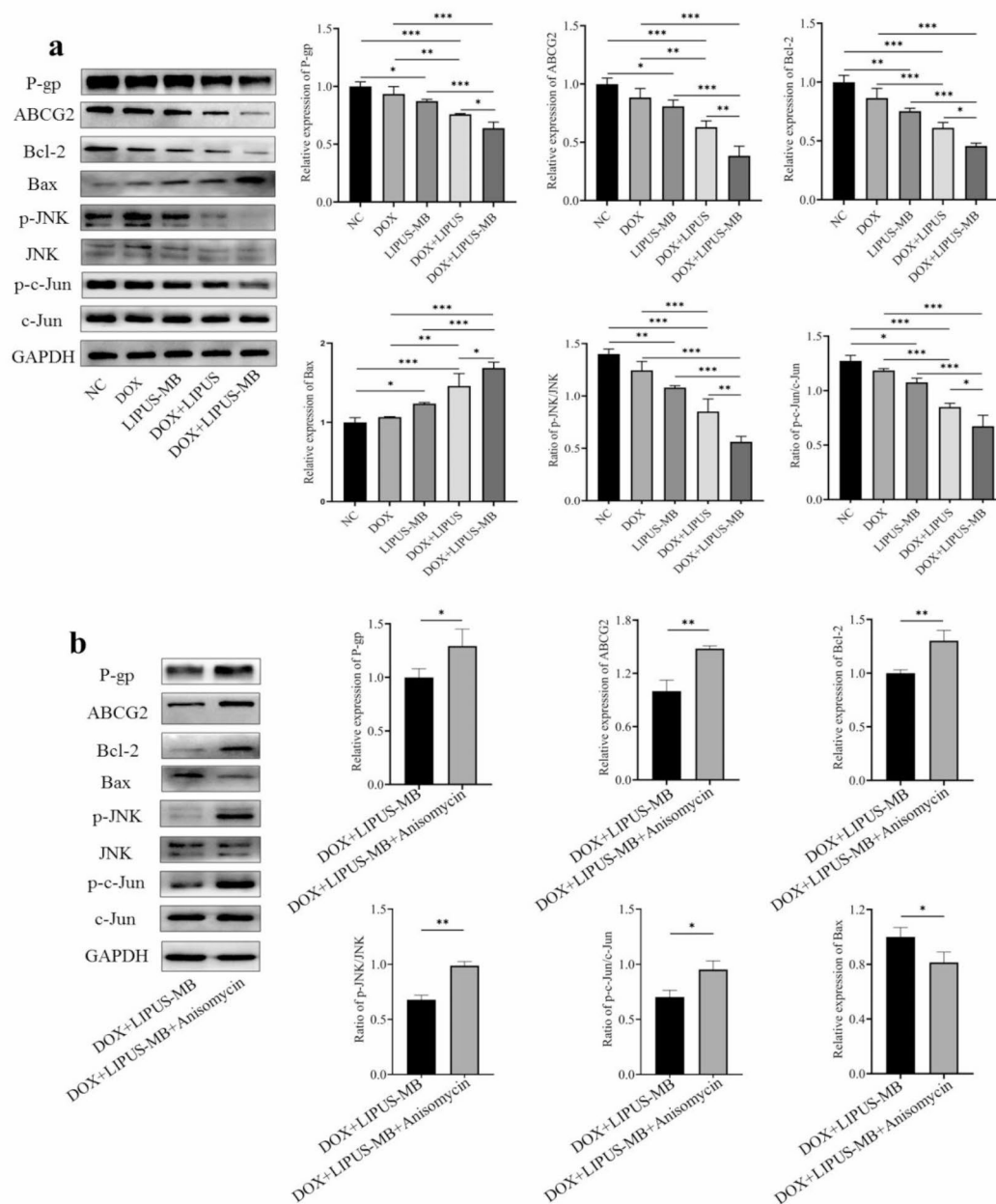
Fig. 3. (**a**) Effect of LIPUS-MB on drug resistance protein, pathways and apoptosis proteins in MDA-MB-231/DOX cells. (**b**) The effect of LIPUS-MB on MDA-MB-231/DOX drug resistance protein, pathways and apoptosis proteins were validated by Anisomycin. GAPDH is the internal parameter. $N = 3$.* $P < 0.05$, ** $P < 0.01$, *** $P < 0.001$. Cropped blots are presented for the sake of clarity and conciseness of data presentation. Uncropped the original blots are presented in the Supplementary data section, as Supplementary Figure S1-S18.

Effect of LIPUS-MB on the expression of relevant proteins in tumor tissues in vivo

The Western blot results (Fig. 6) revealed that the expression of relevant proteins in tumor tissues in vivo following LIPUS-MB treatment was consistent with the expression in vitro. The DOX + LIPUS-MB group exhibited the most significant downregulation of P-gp, ABCG2, p-JNK, p-c-Jun, and Bcl-2 protein expression levels, while demonstrating the highest levels of Bax protein expression ($P < 0.05$). Upon the addition of Anisomycin, the DOX + LIPUS-MB + Anisomycin group showed an upregulation of P-gp, ABCG2, p-JNK, p-c-Jun, and Bcl-2 protein expression levels, accompanied by a downregulation of Bax protein expression levels ($P < 0.05$). These findings suggest that LIPUS-MB, by modulating the JNK/c-Jun pathway, downregulates the expression of P-gp and ABCG2 in tumors, thereby enhancing the anti-tumor effect in vivo and reversing MDR.
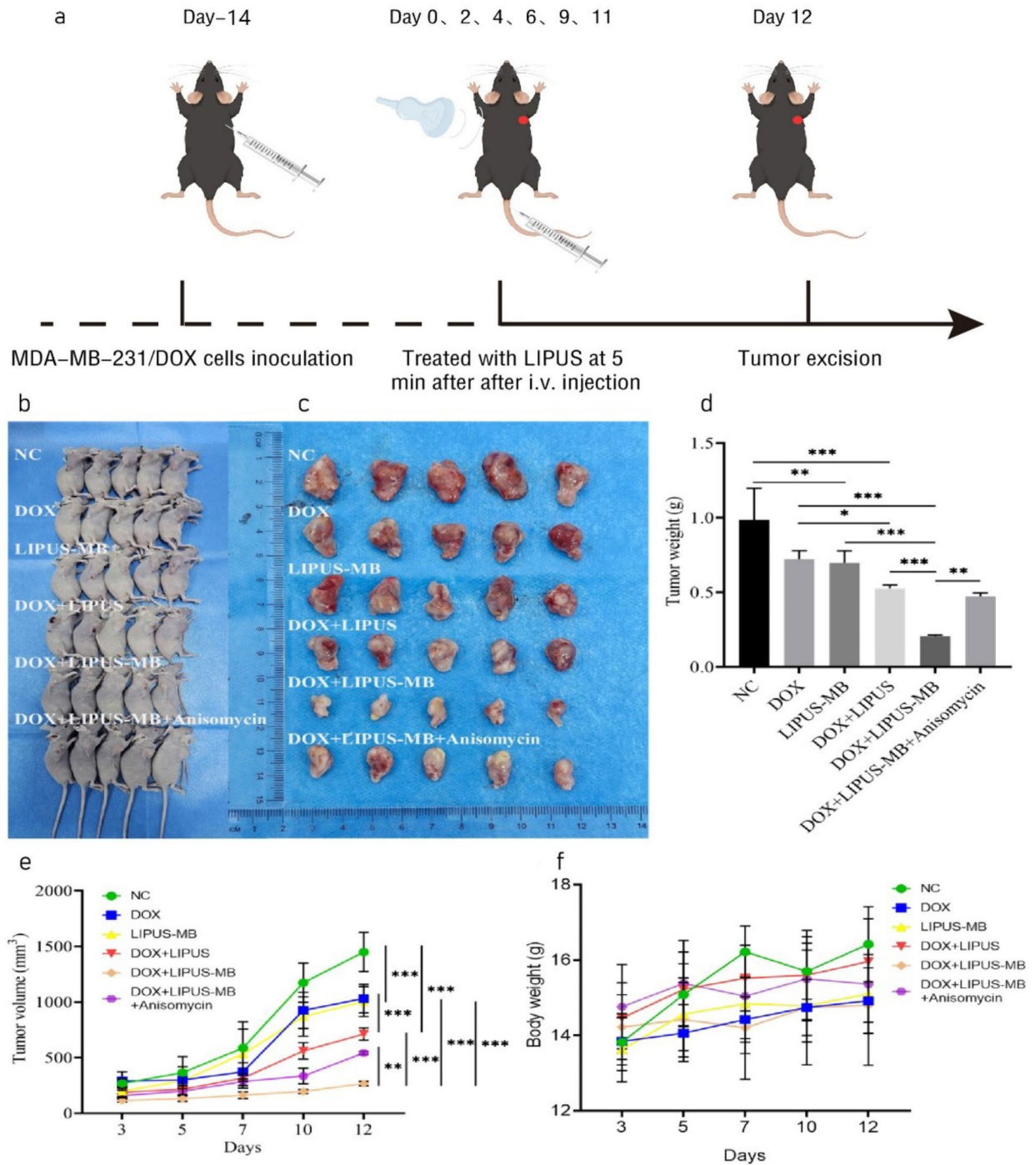
Fig. 4. (**a**) The experimental setup of the animal studies. (**b**) The nude mice, (**c**) Tumor, (**d**) Tumor weight, (**e**) Tumor volume, and (**f**) Weight of mice. $N = 5$, * $P < 0.05$, ** $P < 0.01$, *** $P < 0.001$.

Discussion

As the most aggressive molecular subtype of breast cancer, TNBC is characterized by early onset, advanced clinical stage, high histological grade, and a propensity for local recurrence and metastasis[12]. Currently, TNBC is commonly treated with systemic combination chemotherapy regimens based on anthracyclines, taxanes, and platinum agents, among others, with advancements in prior treatment strategies mostly achieved through optimizing the selection, sequence, and dosing of chemotherapeutic agents[13,14]. The use of neoadjuvant cytotoxic drugs for preoperative chemotherapy is emerging as a promising approach for the systemic treatment of TNBC[15]. However, DOX is widely used as a first-line chemotherapy agent for anthracyclines. Long-term use can lead to
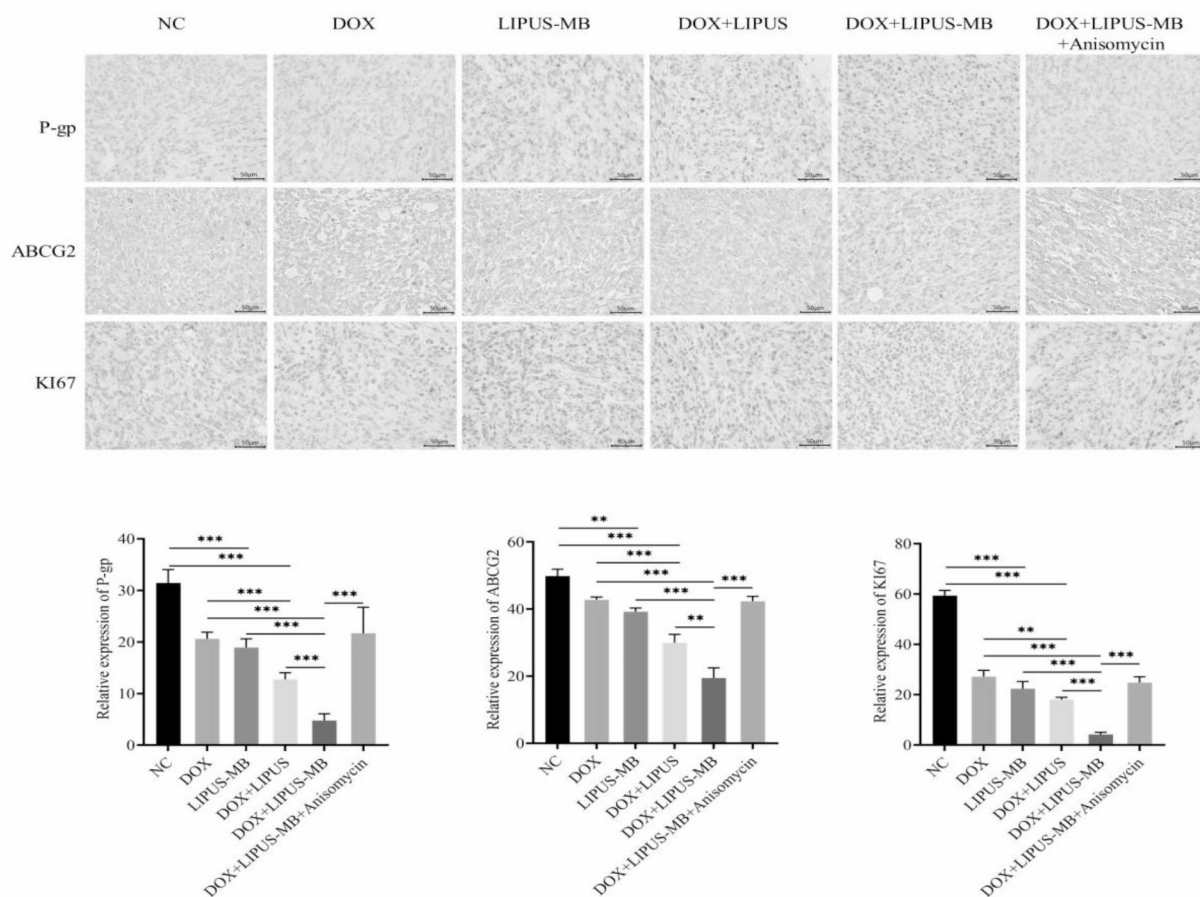
Fig. 5. Immunohistochemical detection of P-gP, ABCG2, KI67. $N = 3$, ** $P < 0.01$, *** $P < 0.001$.

the development of multidrug resistance in tumor cells, resulting in the failure of chemotherapy. Virtually all anti-cancer drugs, including the latest immunotherapies, are constrained by the emergence of drug resistance[16]. There are numerous molecular mechanisms underlying chemoresistance in breast cancer, with the most pivotal being the overexpression of ATP-binding cassette (ABC) transporters. Functioning as efflux transporters with a "drug pump" capability, the transmembrane proteins P-gp and ABCG2 have the ability to bind to a diverse array of chemotherapeutic agents and actively expel them from tumor cells. This process substantially augments the efflux of drugs within tumor cells, ultimately engendering multidrug resistance to commonly employed chemotherapeutic agents[17]. Consequently, the in-depth exploration of molecular targets and therapeutic strategies to reverse TNBC resistance has emerged as a focal point of current research.

Currently, LIPUS-MB has garnered widespread attention in tumor therapy due to its high degree of accuracy and non-invasive nature. The unique biological effects of this approach may offer a promising alternative for reversing MDR. The application of LIPUS in conjunction with MB induces acoustic cavitation, which enhances cell membrane permeability, facilitating the translocation of drugs through biological barriers such as the vascular endothelium and cell membranes to specific sites[18]. Studies have indicated potential mechanisms by which LIPUS in combination with MB enhances transfection efficiency at the cellular level, including the transient formation of micro-pores on the cell membrane, increased membrane fluidity, and facilitation of transmembrane transport[19]. However, the biological effects of LIPUS in combination with MB are subject to the influence of various parameters, such as ultrasound irradiation intensity, microbubble concentration, and cell type. Research suggests that tumor cell lines derived from different tissues can impact the sonoporation effect. Additionally, different acoustic and microbubble parameters can affect cell membrane permeability, and inappropriate parameters, while capable of ablating tumor cells, may also damage surrounding normal tissue cells[20–22].

The preliminary research conducted by our team demonstrated that the different subtypes of breast cancer cell lines have different optimal ultrasound microbubble parameter combinations[23]. Therefore, in this study, we first utilized an orthogonal experimental design to optimize the parameters and investigate the correlation between LIPUS in combination with MB and the sonoporation effect on MDA-MB-231/DOX cells. Our findings
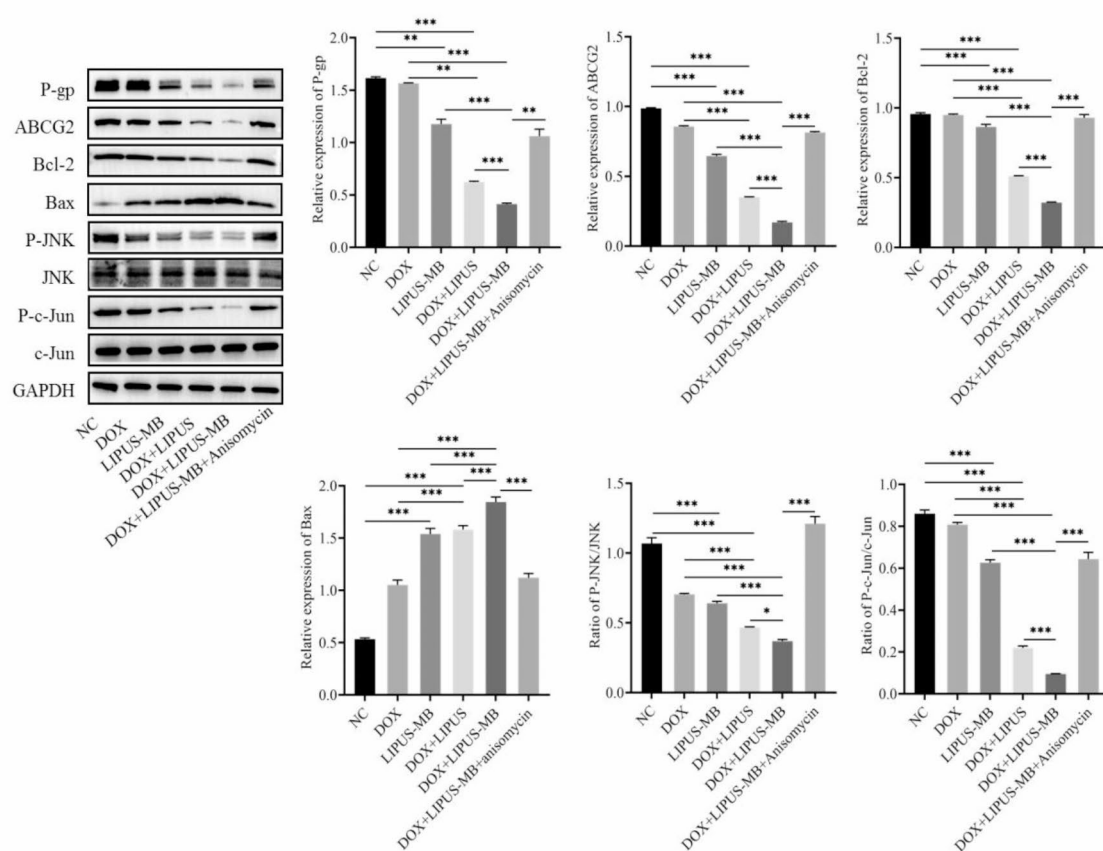
Fig. 6. Effect of LIPUS-MB on P-gP, ABCG2, Bcl-2, Bax, p-JNK, JNK, p-c-Jun, c-Jun on subcutaneous transplantation tumors. $N=3$, * $P < 0.05$, ** $P < 0.01$, *** $P < 0.001$. Cropped blots are presented for the sake of clarity and conciseness of data presentation. Uncropped the original blots are presented in the Supplementary data section, as Supplementary Figure S19-S27.

revealed that the optimal parameters for cells were a microbubble concentration of 20%, ultrasound intensity of 1.0 W/cm^2, and ultrasound irradiation time of 60 s. Under these conditions, LIPUS-MB combined with DOX can enhance the efficiency of drug transfection and the biological effect of ultrasound itself, thereby augmenting the efficacy of chemotherapy. This may offer a targeted therapeutic strategy for TNBC.

Literature has reported[11] that optimized ultrasound microbubble parameters can increase cell transfection efficiency by 9 ~ 16 times. The combination of LIPUS-MB not only effectively inhibits the growth of cancer cells, but also reduces the dosage of DOX required for inducing cell apoptosis, presenting an efficacious approach for combating drug resistance. Furthermore, Qiu demonstrated[24] that LIPUS downregulates the expression of P-gp and ABCG2, thereby enhancing the chemotherapeutic sensitivity of gemcitabine against drug-resistant ASPC-1 pancreatic cancer cells. Moreover, the activation of the JNK/c-Jun pathway has been shown to be associated with multidrug resistance in colon and liver cancers, and the inhibition of the JNK/c-Jun signaling pathway can downregulate the expression of P-gp and ABCG2, thus enhancing the sensitivity of drug-resistant cells to chemotherapy drugs[25,26]. Therefore, this study hypothesizes that the combination of LIPUS with MB can reverse multidrug resistance in TNBC by modulating the JNK/c-Jun pathway to downregulate the expression of P-gp and ABCG2.

The results of this experiment firstly demonstrate that MDA-MB-231/DOX cells exhibit a significantly higher resistance to DOX compared to MDA-MB-231 cells, with a resistance index of 19.17. Following LIPUS-MB treatment, the IC$_{50}$ of MDA-MB-231/DOX cells significantly decreases, indicating a notable reduction

in both cellular resistance and proliferative activity. This suggests that LIPUS-MB effectively enhances the chemotherapeutic sensitivity of cells to DOX, thereby revealing potential underlying mechanisms for reversing multidrug resistance in TNBC.

Furthermore, in order to substantiate the potential link between the reversal of MDR by LIPUS-MB and the inhibition of resistant proteins, Western blotting results reveal that the combination of LIPUS-MB and DOX significantly inhibits the expression of P-gp and ABCG2 proteins in MDA-MB-231/DOX cells. This may be attributed to the detrimental effect of LIPUS-MB on the cellular membrane structure[27], disrupts the conformation of P-gp and ABCG2 proteins embedded within the membrane or alters their intracellular and extracellular distribution, as a result, the reduced expression of P-gp and ABCG2 on the membrane leads to an increased uptake of DOX, consequently reversing the multidrug resistance of the tumor. Conversely, in the DOX + LIPUS-MB + Anisomycin group, there is a noticeable increase in the expression levels of P-gp and ABCG2 proteins, indicating a close association between the multidrug resistance developed by MDA-MB-231/DOX cells and the activation of the JNK/c-Jun pathway.

JNK stands as a pivotal protein kinase within the MAPK signaling cascade, serving as a crucial mediator for the transduction of signals from the cell surface to the nucleus. The JNK/c-Jun pathway is predominantly activated by cytokines and stress responses from the surrounding milieu, participating in the regulation of various biological processes such as tumor proliferation, invasion, migration, apoptosis, and stress responses[28]. Studies have indicated that the activation of the JNK/c-Jun signaling pathway may lead to an upregulation of resistant protein expression in cancer cells, while the inhibition of the JNK/c-Jun signaling pathway by SP600125 (a JNK inhibitor) may potentially impede the development of multidrug resistance[29]. The findings of this study demonstrate that LIPUS in combination with DOX the downregulates the protein expression levels of P-gp, and ABCG2, JNK and c-Jun proteins are dephosphorylated, and following the addition of MB, the protein expression levels of P-gp and ABCG2 are further decreased, the dephosphorylation of JNK and c-Jun proteins was more obvious. This indicates that the activation of the JNK/c-Jun signaling pathway may be essential for inducing MDR. LIPUS-MB partially reverses MDR in MDA-MB-231/DOX cells. Activation of JNK by anisomycin results in a significant increase in the protein expression levels of P-gp and ABCG2. Therefore, the results of this study suggest that LIPUS-MB may partially decreased the expression of drug-resistant protein, reversed multidrug resistance in MDA-MB-231/DOX cells by inhibiting the activation of the JNK pathway.

The apoptosis process of cells is closely related to many signaling pathways, and JNK has a close regulatory role with related apoptotic proteins Bax and Bcl-2[30,31]. The over-expression of Bax can effectively inhibit the expression of Bcl-2, and the imbalance of the two can activate downstream proteins, leading to chromatin condensation and nuclease activation, and further promote cell apoptosis[32]. Research by He et al. has demonstrated that the combination of LIPUS-MB can effectively induce cell death, promote cell apoptosis, and exert significant inhibitory effects on cancer cells[33]. The results of this study demonstrate that the DOX + LIPUS group cell migration was inhibited, induced apoptotic morphological changes, and significantly downregulated the expression of Bcl-2 protein, while upregulating the expression levels of Bax proteins, thereby promoting cellular apoptosis. Additionally, the application of MB on this basis yielded the most pronounced inhibitory effect, resulting in the highest rate of cellular apoptosis. Subsequent reverse validation with Anisomycin revealed an increase in Bcl-2 protein expression levels, accompanied by a decrease in the expression levels of Bax proteins. These findings collectively indicate that LIPUS-MB, through regulation of the JNK/c-Jun pathway, downregulates the expression of P-gp and ABCG2 proteins, thereby inhibiting the growth of MDA-MB-231/DOX cells and promoting cellular apoptosis.

In addition, DOX + LIPUS-MB significantly inhibited the tumor growth in nude mice, and the tumor growth rate and volume were significantly reduced. Immunohistochemical analysis revealed a significant inhibitory effect on the expression of drug-resistant proteins following LIPUS-MB treatment, thereby demonstrating the feasibility of reversing TNBC multidrug resistance. Ki-67 serves as a marker of nuclear proliferation capacity, with heightened expression indicative of actively proliferating cells[34]. The decreased quantity of Ki-67 positive cells in the DOX + LIPUS-MB group suggests LIPUS-MB significantly inhibiting tumor proliferation, promoting apoptosis. Conversely, the increased quantity of Ki-67 positive cells in the DOX + LIPUS-MB + Anisomycin group suggests that activation of the JNK/c-Jun pathway can exert an inhibitory effect on cellular apoptosis. Consistent with the in vitro findings, in vivo Western blot results further substantiate the role of LIPUS-MB in downregulating the expression of P-gp and ABCG2 proteins through the JNK/c-Jun pathway, thereby inhibiting cellular proliferation, migration, and promoting apoptosis, consequently enhancing the in vivo anti-tumor effects of DOX and partially reversing MDR of doxorubicin in TNBC.

In conclusion, this study employed an orthogonal experimental design to screen for the optimal combination of LIPUS-MB parameters, which effectively reversed the multidrug resistance in TNBC. LIPUS-MB downregulated the expression of P-gp and ABCG2 proteins both in vitro and in vivo, thereby inhibiting cell proliferation, inducing morphological changes in cells and promoting apoptosis. These effects were closely associated with the inhibition of the JNK/c-Jun signaling pathway. This investigation elucidated the role and mechanism of LIPUS-MB in reversing chemoresistance in TNBC MDA-MB-231/DOX cells. Furthermore, it demonstrated the therapeutic efficacy of the combined application of LIPUS-MB and DOX in xenograft tumors in nude mice. These findings not only contribute to the understanding of novel therapeutic approaches but also provide a new avenue for the clinical management of drug-resistant TNBC. However, the mechanism by which LIPUS-MB combined with DOX reverses TNBC drug resistance may be related to many aspects such as cell type, endothelium, and tumor microenvironment[35], so our team will further explore in the future.

Methods
Materials
Cells

Human breast cancer MDA-MB-231 cell line and MDA-MB-231/DOX cell line, they were purchased from the Shanghai Institute of Cell and Biology, Chinese Academy of Sciences.

Experimental animals

BALB/c nude mice were purchased from the Beijing SPF Biological Co., LTD. Relevant animal experiments were approved by the Experimental Animal Ethics Committee of Yantai Yuhuangding Hospital (2024−256). We confirm that all experiments were performed in accordance with relevant named guidelines and regulations. And we confirm that the authors complied with the ARRIVE guidelines.

Main reagents

DOX, purity > 98.0%, FITC-Dextran 500 (Sigma Company, USA); fetal bovine serum (PAN Company, German); DMEM cell culture medium, RPMI 1640 cell culture medium, 0.25% trypsin digestion liquid, penicillin-streptomycin mixture (Shandong Sparkjade Biotech Co.,Ltd., China); CCK-8 kit (China Anhui Biosharp Life Science& Technology Co.,Ltd., China); Hoechst 33,342 Living Cell Staining Solution (Shanghai Beyotime Biotech Co.,Ltd., China); Annexin V-FITC/PI Apoptosis Detection Kit (Wuhan Procell Life Science& Technology Co.,Ltd., China). P-gp rabbit monoclonal antibody, c-Jun rabbit monoclonal antibody, phospho-c-Jun rabbit polyclonal antibody, Anisomycin (JNK activator) (Shanghai Beyotime Biotech Co.,Ltd., China), ABCG2 Ab, Ki67 (Affinity Bioscience, USA), Rabbit anti-JNK polyclonal antibody, Rabbit anti-phospho-JNK polyclonal antibody (Beijing Bioss Co.,Ltd., China), Bcl-2 rabbit mAb (Wuhan ABclonal Technology Co.,Ltd.,China), Bax antibody (Shanghai Abways Technology Co.,Ltd., China), Anti-GAPDH antibody, HRP Tagged Goat Anti-Rabbit IgG (H + L) (Shanghai, BBI Life Sciences Co.,Ltd., China); The relevant reagents required for Western blot experiments are from Shandong Sparkjade Biotech Co.,Ltd, China.

Cell culture

MDA-MB-231 and MDA-MB-231/DOX cells were thawed and centrifuged at 1000r/min for 5 min. The former was seeded in DMEM culture medium containing 10% fetal bovine serum and 1% Penicillin-Streptomycin Solution while the latter was seeded in RPMI 1640 medium containing 10% fetal bovine serum and 1% Penicillin-Streptomycin Solution (hereinafter referred to as complete culture medium). The cells were placed in a 37℃, 5% CO_2 cell culture incubator for recovery and growth to normal cell state. Subsequently, 1μM DOX was added to the MDA-MB-231/DOX cells to maintain drug resistance, and the cells were passaged every 2~3 days. Cells in the logarithmic growth phase were collected for experiments.

Experimental facilities of ultrasound

The therapeutic ultrasound apparatus WED-101 (Welld Medical Electronics Co.,Ltd, China), diameter of its planar transducer of 45 mm, with a working frequency of 1 MHz, duty cycle 60% and pulse repetition frequency of 100 Hz were used in this study. SonoVue (Bracco Suisse SA, China) was prepared by reconstituting the powder with 5 ml sodium chloride 0.9% w/v solution. The ultrasound transducer was placed on the bottom of the Petri dish with the probe facing up, and coupler was applied to maintain a distance of 1 cm between the transducer and the Petri dish (Fig. 2a).

Determination of the optimal LIPUS-MB parameters by orthogonal analysis

Three factors, including microbubble concentration, ultrasound intensity, and irradiation time, were selected at different levels (microbubble contrast agent concentration: 10%, 20%, 30%; ultrasound intensity: 0.5 W/cm², 1.0 W/cm², 1.5 W/cm²; irradiation time: 30s, 60s, 90s). Design the experimental scheme of L9 (3³) orthogonal array (Table 2). MDA-MB-231/DOX cells were treated according to the established experimental protocol to mediate the intracellular transport of FITC-Dextran 500 (FD500), a model drug[23]. Using the cell sonoporation effect and cell survival rate as indicators, the sum of the experimental indicators for the m level of the j column of each parameter (K_{jm}) was calculated, as well as the average experimental indicator for each parameter (k_{jm}).

Test no.	Factors		
	Microbubble concentration(%)	Sound intensity(W/cm²)	Irradiation time(s)
1	30	1.5	30
2	10	1.0	90
3	30	0.5	90
4	10	1.5	60
5	20	1.5	90
6	30	1.0	60
7	20	1.0	90
8	20	0.5	60
9	10	0.5	30

Table 2. Orthogonal experimental design.

Subsequently, K_{jm} and k_{jm} were calculated, and the optimal level of each parameter was determined, the range value R (k_{max}-k_{min}) was also calculated to determine the primary and secondary effects of the three parameters on drug-resistant cell lines. By synthesizing K_{jm}, k_{jm}, and R values, the optimal parameter combination for LIPUS-MB on MDA-MB-231/DOX cells was ultimately determined.

Detection of cell drug resistance by CCK-8
The logarithmic growth phase MDA-MB-231 cells and MDA-MB-231/DOX cells were separately digested with 0.25% trypsin to prepare single cell suspensions, with a cell concentration of 1×10^4cells/mL. These suspensions were then seeded in a 96-well plate (100μL/well), with 5 replicates for each group and set blank group at the same time. After incubation in complete culture medium containing different final concentrations (10^{-2}μM, 10^{-1}μM, 10^0μM, 10^1μM, 10^2μM, 10^3μM) of DOX for 24 h, 10μL of CCK-8 solution was added to each well and further incubated for 2 h. The OD at 450 nm of each well was measured using a microplate reader.

$$\text{Cell survival rate} = \frac{\text{OD}_{\text{LIPUS - MB group}} - \text{OD}_{\text{blank group}}}{\text{OD}_{\text{control group}} - \text{OD}_{\text{blank group}}} \times 100\%$$

A drug inhibition curve was plotted, and the IC_{50} values for MDA-MB-231 and MDA-MB-231/DOX cells were calculated.

$$\text{Resistance index (RI)} = \frac{IC_{50} \text{ MDA - MB - 231/DOX}}{IC_{50} \text{ MDA - MB - 231}}$$

Evaluating the reversal efficacy of LIPUS-MB
Cells in the logarithmic growth phase were prepared as single cell suspensions and divided into the LIPUS-MB treatment group and the untreated group. Following treatment, the cells were collected and adjusted to a concentration of 1×10^4 cells/mL. The subsequent steps were consistent with the experimental methods of CCK-8 in the previous section. The proliferation activity of cells in each group was evaluated, and the impact of LIPUS-MB on the IC_{50} of drug-resistant cells was calculated.

$$\text{Resistance reversal index} = \frac{IC_{50} \text{ untreated group}}{IC_{50} \text{ LIPUS-MB treatment group}}$$

$$\text{Relative reversal efficiency} = \frac{IC_{50}\text{MDA} - \text{MB} - 231/\text{DOX} - IC_{50}\text{LIPUS} - \text{MB treatment group}}{IC_{50}\text{MDA} - \text{MB} - 231/\text{DOX} - IC_{50}\text{MDA} - \text{MB} - 231} \times 100\%$$

Treatment groups
MDA-MB-231/DOX cells were divided into five groups: NC group (without treatment), DOX group (treated with 5μM DOX), LIPUS-MB group (treated with 1.0 W/cm² ultrasound, and 60s, 20% microbubbles), DOX+LIPUS group (treated with 1.0 W/cm² ultrasound, 60s and 5μM DOX), DOX+LIPUS-MB group (treated with 1.0 W/cm² ultrasound, 60s, and 20% microbubbles and 5μM DOX).

Detection of cell chromatin condensation by hoechst33342 staining
The cells treated in each group were seeded into 12-well plates at a volume of 1mL per well, ensuring even distribution. After 24 h, the old culture medium was removed, and the cells were washed twice with PBS. Subsequently, 10 μl of Hoechst 33,342 live cell staining solution (40×) was added to each well. The cells were then incubated in a sterile incubator for an additional 10 min before being washed 2~3 times with PBS. The staining was then visualized and recorded under a fluorescence inverted microscope.

Detection of apoptosis by Annexin VFITC /PI staining
The cells treated in each group were seeded into 6-well plates and after 24 h, they were subjected to trypsin digestion. The cell concentration was then adjusted to 5×10^5cells/mL and resuspended in 500μL of Binding Buffer. Subsequently, 5μL of Annexin V-FITC and 5μL of PI were added sequentially and mixed well. The cells were then incubated in the dark for 15 min, followed by detection of the apoptosis rate using flow cytometry.

Detection of drug resistance, pathways and apoptosis protein expression by Western blot
Cells were continued to be cultured in the incubation chamber for 24 h following experimental treatment, subsequently the treated cells from each group were lysed in RIPA buffer containing PMSF to extract total protein. Quantification of western blot signals was performed using an ultramicrospectrophotometer. After denaturation, proteins were subjected to SDS-PAGE, transmembrane, and blocked. P-gp rabbit monoclonal antibody, ABCG2 Ab, Rabbit anti-JNK polyclonal antibody, Rabbit anti-phospho-JNK polyclonal antibody, c-Jun rabbit monoclonal antibody, phospho-c-Jun rabbit polyclonal antibody, Bcl-2 rabbit mAb, Bax antibody (the dilution concentration of the above antibodies was 1:1000) and Anti-GAPDH antibody (1:4000) primary antibody were incubated at 4℃ overnight, and after washing the membrane, HRP Tagged Goat Anti-Rabbit IgG (H+L) (1:5000) was added and incubated for 1 h on a shaker. After washing the membrane again, ECL luminescent solution was added for development and photography, and the results were analyzed by chemiluminescence system.

Establishment of transplant tumor animal model
Healthy BALB/c nude mice, aged 6–8 weeks and weighing 20–25 g, were housed under specific pathogen-free (SPF) conditions, with a temperature of 23–25 °C, relative humidity of 40–70%, and alternating day and night light cycles, with food and water available ad libitum. MDA-MB-231/DOX cells were enzymatically digested to prepare a cell suspension at a concentration of 1×10^7 cells/mL, and 0.1 mL (1×10^6 cells) was subcutaneously injected into the right axilla of each mouse. Two weeks after inoculation, the tumor volume reached 100–300 mm³. At this point, 30 mice were selected and grouped according to tumor volume, ensuring no significant difference in overall tumor volume between groups. The mice were fixed on the workbench, anesthetized with 3% sodium pentobarbital via intraperitoneal injection, treated according to the experimental protocol. Tumor growth was monitored 24 h after each treatment. At the end of the experiment, after anesthetized with 3% sodium pentobarbital, the cervical vertebrae of nude mice were dislocated and sacrificed, and the transplanted tumors were isolated and weighed (Figure 4a).

Thirty BALB/c nude mice were randomly divided into six groups: NC group (untreated), DOX group (intraperitoneal injection with 3.0 mg/kg DOX), LIPUS-MB group (1.0 W/cm^2 ultrasound, 5 min, tail vein injection with 20% microbubbles), DOX + LIPUS group (intraperitoneal injection with 3.0 mg/kg DOX + 1.0 W/cm^2 ultrasound, 5 min), DOX + LIPUS-MB group (intraperitoneal injection with 3.0 mg/kg DOX + 1.0 W/cm^2 ultrasound, 5 min, tail vein injection with 20% microbubbles), and DOX + LIPUS-MB + Anisomycin group (intraperitoneal injection with 3.0 mg/kg DOX + 1.0 W/cm^2 ultrasound, 5 min, tail vein injection with 20% microbubbles + 4 µg/kg Anisomycin). Anisomycin could activate JNK phosphorylation, the group was added to reverse verify the effect of LIPUS-MB on JNK/c-Jun pathway related proteins, with 5 mice in each group. Tumor volumes were calculated using the following formula: $V = ab^2/2$, where a and b are the long and short diameters, respectively.

Immunohistochemical analysis
Tumor tissues were fixed in 4% paraformaldehyde, embedded in paraffin, and sectioned (5 µm). After successively dewaxed rehydration, incubated with antigen retrieval solution, processed with hydrogen peroxide to block endogenous peroxidase activity and blocked with 4% normal goat serum. The tissue sections were incubated with P-gp (1:100), ABCG2 (1:100), and Ki67 antibodies (1:40) at 4 °C overnight. PBS scoured tissue sections, polymerized HRP- labeled anti-rabbit IgGII antibody incubated for 45 min in the chamber, PBS scoured tissue sections again, and then stained with hematoxylin and DAB for color development. Positive results were identified by brown or brownish-yellow nuclear staining. Ki67, P-gp and ABCG2 expression were evaluated using Image J software to calculate the average optical density (AOD) of immunohistochemical images.

Detection of tumor tissues drug resistance, pathways and apoptosis protein expression by Western blot
50 mg of tumor tissue was homogenized in RIPA lysis buffer containing PMSF using a homogenizer to extract total protein. Following the procedure as described western blot in vitro, the expression levels of P-gp, ABCG2, JNK, p-JNK, c-Jun, p-c-Jun, Bcl-2, Bax proteins were evaluated.

Statistical analysis
GrapdhPad 9.0 was used for data processing and mapping. The measurement data were represented by mean ± standard deviation ($\bar{x} \pm s$). *t*-test was used for comparison between two independent sample groups, one-way analysis of variance was used for comparison between multiple groups, and Tukey-*t* test was used for multiple comparison between groups. Dunnet-*t* test was used to compare the experimental group with the control group. $P < 0.05$ was considered statistically significant.

Data availability
The datasets generated during and/or analysed during the current study are available from the corresponding author on reasonable request.

References
1. Siegel, R. L., Miller, K. D., Wagle, N. S., Jemal, A. & Cancer statistics *CA: A Cancer Journal For Clinicians.* 73(1), 17–48 (2023). (2023).
2. Nolan, E., Lindeman, G. J. & Visvader, J. E. Deciphering breast cancer: from biology to the clinic. *Cell.* **186** (8), 1708–1728 (2023).
3. Yuan, S. J. et al. Doxorubicin-polyglycerol-nanodiamond conjugate is a cytostatic agent that evades chemoresistance and reverses cancer-induced immunosuppression in triple-negative breast cancer. *J. Nanobiotechnol.* **17** (1), 110. https://doi.org/10.1186/s12951-019-0541-8 (2019).
4. Fan, J., To, K. K. W., Chen, Z. S. & Fu, L. ABC transporters affects tumor immune microenvironment to regulate cancer immunotherapy and multidrug resistance. *Drug Resist. Updates: Reviews Commentaries Antimicrob. Anticancer Chemother.* **66**, 100905. https://doi.org/10.1016/j.drup.2022.100905 (2023).
5. Zeng, Z. et al. Novel Sigma-2 receptor ligand A011 overcomes MDR in adriamycin-resistant human breast cancer cells by modulating ABCB1 and ABCG2 transporter function. *Front. Pharmacol.* **13**, 952980. https://doi.org/10.3389/fphar.2022.952980 (2022).
6. Kumar, H. et al. A review of biological targets and therapeutic approaches in the management of triple-negative breast cancer. *J. Adv. Res.* **54**, 271–292 (2023).
7. Jiang, X. et al. A review of low-intensity pulsed Ultrasound for Therapeutic Applications. *IEEE Trans. Bio Med. Eng.* **66** (10), 2704–2718 (2019).
8. Wanigasekara, J., de Carvalho, A. M. A., Cullen, P. J., Tiwari, B. & Curtin, J. F. Converging technologies: targeting the hallmarks of cancer using ultrasound and microbubbles. *Trends Cancer.* **7** (10), 886–890 (2021).

9. Zhang, L. et al. Cascade Drug Delivery through Tumor barriers of Pancreatic Cancer *via* Ultrasound in Combination with Functional Microbubbles. *ACS Biomaterials Sci. Eng.* **8** (4), 1583–1595 (2022).

10. Luo, H. et al. Ultrasonic irradiation and SonoVue microbubbles-mediated RNA interference targeting PRR11 inhibits breast cancer cells proliferation and metastasis, but promotes apoptosis. *Biosci. Rep.* **40** (11), BSR20201854. https://doi.org/10.1042/BSR20201854 (2020).

11. Chowdhury, S. M. et al. Longitudinal assessment of ultrasound-guided complementary microRNA therapy of hepatocellular carcinoma. *J. Controlled Release: Official J. Controlled Release Soc.* **281**, 19–28 (2018).

12. Huang, M. et al. Economic and Humanistic Burden of Triple-negative breast Cancer: a systematic literature review. *PharmacoEconomics.* **40** (5), 519–558 (2022).

13. Yin, L., Duan, J. J., Bian, X. W. & Yu, S. C. Triple-negative breast cancer molecular subtyping and treatment progress. *Breast Cancer Research: BCR.* **22** (1), 61. https://doi.org/10.1186/s13058-020-01296-5 (2020).

14. Leon-Ferre, R. A. & Goetz, M. P. Advances in systemic therapies for triple negative breast cancer. *BMJ (Clinical Res. Ed).* **381**, e071674. https://doi.org/10.1136/bmj-2022-071674 (2023).

15. Tamirisa, N., Hunt, K. K., Neoadjuvant & Chemotherapy Endocrine therapy, and targeted therapy for breast Cancer: ASCO Guideline. *Ann. Surg. Oncol.* **29** (3), 1489–1492 (2022).

16. Craig, M., Jenner, A. L., Namgung, B., Lee, L. P. & Goldman, A. Engineering in Medicine to address the challenge of Cancer Drug Resistance: from Micro- and nanotechnologies to Computational and Mathematical modeling. *Chem. Rev.* **121** (6), 3352–3389 (2021).

17. Amawi, H., Sim, H. M., Tiwari, A. K., Ambudkar, S. V. & Shukla, S. ABC transporter-mediated Multidrug-Resistant Cancer. *Adv. Exp. Med. Biol.* **1141**, 549–580 (2019).

18. Zattoni, I. F. et al. Targeting breast cancer resistance protein (BCRP/ABCG2): functional inhibitors and expression modulators. *Eur. J. Med. Chem.* **237**, 114346. https://doi.org/10.1016/j.ejmech.2022.114346 (2022).

19. Meng, L. et al. Sonoporation of Cells by a Parallel Stable Cavitation Microbubble Array. *Advanced Science (Weinheim, Baden-Wurttemberg, Germany).* 6(17), 1900557; (2019). https://doi.org/10.1002/advs.201900557

20. Shi, D. et al. Influence of tumor cell lines derived from different tissue on sonoporation efficiency under ultrasound microbubble treatment. *Ultrason. Sonochem.* **38**, 598–603 (2017).

21. Wang, M. et al. Sonoporation-induced cell membrane permeabilization and cytoskeleton disassembly at varied acoustic and microbubble-cell parameters. *Sci. Rep.* **8** (1), 3885. https://doi.org/10.1038/s41598-018-22056-8 (2018).

22. Yang, Y., Li, Q., Guo, X., Tu, J. & Zhang, D. Mechanisms underlying sonoporation: Interaction between microbubbles and cells. *Ultrason. Sonochem.* **67**, 105096. https://doi.org/10.1016/j.ultsonch.2020.105096 (2020).

23. Qu, N. et al. Breast Cancer cell line phenotype affects Sonoporation Efficiency under Optimal Ultrasound Microbubble conditions. *Med. Sci. Monitor: Int. Med. J. Experimental Clin. Res.* **24**, 9054–9062 (2018).

24. Qiu, F., Chen, J., Cao, J., Diao, F. & Huang, P. Lowintensity lowfrequency ultrasound enhances the chemosensitivity of gemcitabineresistant ASPC-1 cells via PI3K/AKT/NFκB pathwaymediated ABC transporters. *Oncol. Rep.* **44** (3), 1158–1168 (2020).

25. Zhu, M. M. et al. Increased JNK1 signaling pathway is responsible for ABCG2-mediated multidrug resistance in human colon cancer. *PloS One.* **7** (8), e41763. https://doi.org/10.1371/journal.pone.0041763 (2012).

26. Liu, X. Y., Liu, S. P., Jiang, J., Zhang, X. & Zhang, T. Inhibition of the JNK signaling pathway increases sensitivity of hepatocellular carcinoma cells to cisplatin by down-regulating expression of P-glycoprotein. *Eur. Rev. Med. Pharmacol. Sci.* **20** (6), 1098–1108 (2016).

27. Alatrash, G., Jakher, H., Stafford, P. D. & Mittendorf, E. A. Cancer immunotherapies, their safety and toxicity. *Exp. Opin. Drug Saf.* **12** (5), 631–645 (2013).

28. Wu, Q. et al. Selective inhibitors for JNK signalling: a potential targeted therapy in cancer. *J. Enzyme Inhib. Med. Chem.* **35** (1), 574–583 (2020).

29. Wang, P. P. et al. Astragaloside IV downregulates the expression of MDR1 in Bel-7402/FU human hepatic cancer cells by inhibiting the JNK/cJun/AP-1 signaling pathway. *Mol. Med. Rep.* **16** (3), 2761–2766 (2017).

30. Huang, Y. C., Pan, W., Li, H. & Yan, T. c-Jun NH2-terminal kinase suppression significantly inhibits the growth of transplanted breast tumors in mice. *J. Int. Med. Res.* **48** (6), 300060520929858. https://doi.org/10.1177/0300060520929858 (2020).

31. Wu, Q. et al. JNK signaling in cancer cell survival. *Med. Res. Rev.* **39** (6), 2082–2104 (2019).

32. Lin, K. N., Zhao, W., Huang, S. Y. & Li, H. Grape seed proanthocyanidin extract induces apoptosis of HL-60/ADR cells via the Bax/Bcl-2 caspase-3/9 signaling pathway. *Translational Cancer Res.* **10** (9), 3939–3947 (2021).

33. He, M. et al. Ultrasound-activatable g-C_3N_4-Anchored Titania Heterojunction as an intracellular redox Homeostasis Perturbator for Augmented Oncotherapy. *Small (Weinheim Der Bergstrasse Germany).* **19** (21), e2300244. https://doi.org/10.1002/smll.202300244 (2023).

34. Remnant, L., Kochanova, N. Y., Reid, C., Cisneros-Soberanis, F. & Earnshaw, W. C. The intrinsically disorderly story of Ki-67. *Open. Biology.* **11** (8), 210120. https://doi.org/10.1098/rsob.210120 (2021).

35. Presset, A. et al. Endothelial cells, First Target of Drug Delivery using Microbubble-assisted Ultrasound. *Ultrasound. Med. Biol.* **46** (7), 1565–1583 (2020).

Acknowledgements

Author contributions

QNN and WZH designed, conceived the study, and performed experiments. MQK wrote the main manuscript text. BML and LHX prepared figures and tables. All authors participated in the data analysis and writing of the initial draft. CXL and LYQ were involved in revising the manuscript critically for important intellectual content. All authors read and approved the final manuscript. QNN and WZH contributed equally to this work and should be regarded as co-first authors.

Funding

Declarations

Competing interests

The authors declare no competing interests.

Additional information

Supplementary Information The online version contains supplementary material available at https://doi.org/10.1038/s41598-024-78272-y.

Correspondence and requests for materials should be addressed to X.C.

Reprints and permissions information is available at www.nature.com/reprints.

Publisher's note Springer Nature remains neutral with regard to jurisdictional claims in published maps and institutional affiliations.